

DeepSynth: Automata Synthesis for Automatic Task Segmentation in Deep Reinforcement Learning [Extended Version]

Mohammadhosein Hasanbeig, Natasha Yogananda Jeppu,
Alessandro Abate, Tom Melham, Daniel Kroening*

Computer Science Department, University of Oxford, Parks Road, Oxford, United Kingdom, OX1 3QD
{hosein.hasanbeig, natasha.yogananda.jeppu, alessandro.abate, tom.melham}@cs.ox.ac.uk and daniel.kroening@magd.ox.ac.uk

Abstract

This paper proposes DeepSynth, a method for effective training of deep Reinforcement Learning (RL) agents when the reward is sparse and non-Markovian, but at the same time progress towards the reward requires achieving an unknown *sequence* of high-level objectives. Our method employs a novel algorithm for synthesis of compact automata to uncover this sequential structure automatically. We synthesise a human-interpretable automaton from trace data collected by exploring the environment. The state space of the environment is then enriched with the synthesised automaton so that the generation of a control policy by deep RL is guided by the discovered structure encoded in the automaton. The proposed approach is able to cope with both high-dimensional, low-level features and unknown sparse non-Markovian rewards. We have evaluated DeepSynth’s performance in a set of experiments that includes the Atari game *Montezuma’s Revenge*. Compared to existing approaches, we obtain a reduction of *two* orders of magnitude in the number of iterations required for policy synthesis, and also a significant improvement in scalability.

1 Introduction

Reinforcement Learning (RL) is the key enabling technique for a variety of applications of artificial intelligence, including advanced robotics (Polydoros and Nalpanitidis 2017), resource and traffic management (Mao et al. 2016; Sadigh et al. 2014), drone control (Abbeel et al. 2007), chemical engineering (Zhou et al. 2017), and gaming (Mnih et al. 2015). While RL is a very general architecture, many advances in the last decade have been achieved using specific instances of RL that employ a deep neural network to synthesise optimal policies. A deep RL algorithm, AlphaGo (Silver et al. 2016), played moves in the game of Go that were initially considered glitches by human experts, but secured victory against the world champion. Similarly, AlphaStar (Vinyals et al. 2019) was able to defeat the world’s best players at the real-time strategy game StarCraft II, and to reach top 0.2% in scoreboards with an “unimaginably unusual” playing style.

While deep RL can autonomously solve many problems in complex environments, tasks that feature extremely sparse, non-Markovian rewards or other long-term sequential structures are often difficult or impossible to solve by unaided RL.

A well-known example is the Atari game *Montezuma’s Revenge*, in which DQN (Mnih et al. 2015) failed to score. Interestingly, *Montezuma’s Revenge* and other hard problems often require learning to accomplish, possibly in a specific sequence, a set of high-level objectives to obtain the reward. These objectives can often be identified with passing through designated and semantically distinguished states of the system. This insight can be leveraged to obtain a manageable, high-level model of the system’s behaviour and its dynamics.

Contribution: In this paper we propose DeepSynth, a new algorithm that automatically infers unknown sequential dependencies of a reward on high-level objectives and exploits this to guide a deep RL agent when the reward signal is history-dependent and significantly delayed. We assume that these sequential dependencies have a *regular* nature, in formal language theory sense (Gulwani 2012). The identification of dependency on a sequence of high-level objectives is the key to breaking down a complex task into a series of Markovian ones. In our work, we use automata expressed in terms of high-level objectives to orchestrate sequencing of low-level actions in deep RL and to guide the learning towards sparse rewards. Furthermore, the automata representation allows a human observer to easily interpret the deep RL solution in a high-level manner, and to gain more insight into the optimality of that solution.

At the heart of DeepSynth is a *model-free* deep RL algorithm that is synchronised in a closed-loop fashion with an automaton inference algorithm, enabling our method to learn a policy that discovers and follows high-level sparse-reward structures. The synchronisation is achieved by a product construction that creates a hybrid architecture for the deep RL. When dealing with raw image input, we assume that an off-the-shelf unsupervised image segmentation method, e.g. (Liu et al. 2019), can provide enough object candidates in order to identify semantically distinguished states. We evaluate the performance of DeepSynth on a selection of benchmarks with unknown sequential high-level structures. These experiments show that DeepSynth is able to automatically discover and formalise unknown, sparse, and non-Markovian high-level reward structures, and then to efficiently synthesise successful policies in various domains where other related approaches fail. DeepSynth represents a better integration of deep RL and formal automata synthesis than previous approaches, making learning for non-Markovian rewards more scalable.

*The work in this paper was done prior to joining Amazon.

2 Related Work

Our research employs formal methods to deal with the sparse reward problem in RL. In the RL literature, the dependency of rewards on objectives is often tackled with *options* (Sutton and Barto 1998), or, in general, the dependencies are structured *hierarchically*. Current approaches to Hierarchical RL (HRL) very much depend on state representations and whether they are structured enough for a suitable reward signal to be effectively engineered manually. HRL therefore often requires detailed supervision in the form of explicitly specified high-level actions or intermediate supervisory signals (Precup 2001; Kearns and Singh 2002; Daniel, Neumann, and Peters 2012; Kulkarni et al. 2016; Vezhnevets et al. 2016; Bacon, Harb, and Precup 2017). A key difference between our approach and HRL is that our method produces a modular, human-interpretable and succinct graph to represent the sequence of tasks, as opposed to complex and comparatively sample-inefficient structures, e.g. RNNs.

The closest line of work to ours, which aims to avoid HRL requirements, are model-based (Fu and Topcu 2014; Sadigh et al. 2014; Fulton and Platzer 2018; Cai et al. 2021) or model-free RL approaches that constrain the agent with a temporal logic property (Hasanbeig, Abate, and Kroening 2018; Toro Icarte et al. 2018; Camacho et al. 2019; Hasanbeig et al. 2019a; Yuan et al. 2019; De Giacomo et al. 2019, 2020; Hasanbeig, Abate, and Kroening 2019b,a, 2020; Hasanbeig, Kroening, and Abate 2020; Kazemi and Soudjani 2020; Lavaei et al. 2020). These approaches are limited to finite-state systems, or more importantly require the temporal logic formula to be known a priori. The latter assumption is relaxed in (Toro Icarte et al. 2019; Rens et al. 2020; Rens and Raskin 2020; Furelos-Blanco et al. 2020; Gaon and Brafman 2020; Xu et al. 2020), by inferring automata from exploration traces.

Automata inference in (Toro Icarte et al. 2019) uses a local-search based algorithm, Tabu search (Glover and Laguna 1998). The automata inference algorithm that we employ uses SAT, where the underlying search algorithm is a backtracking search method called DPLL (Davis and Putnam 1960). In comparison with Tabu search, the DPLL algorithm is complete and explores the entire search space efficiently (Cook and Mitchell 1996), producing more accurate representations of the trace. A detailed comparison of the two approaches is provided in Section B of the Appendix. The Answer Set Programming (ASP) based algorithm used to learn automata in (Furelos-Blanco et al. 2020), also uses DPLL but assumes a known upper bound for the maximum finite distance between automaton states. We further relax this restriction and assume that the task and its automaton are entirely unknown.

A classic automata learning technique is the L^* algorithm (Angluin 1987). This is used to infer automata in (Rens et al. 2020; Rens and Raskin 2020; Gaon and Brafman 2020; Chockler et al. 2020). It employs a series of equivalence and membership queries from an oracle, the results of which are used to construct the automaton. The absence of an oracle in our setting prevents the use of L^* in our method.

Another common approach for synthesising automata from traces is *state-merge* (Biermann and Feldman 1972a). Variants of the state-merge algorithm, e.g. Evidence-Driven State

Merge (EDSM) (Lang, Pearlmutter, and Price 1998), use both positive and negative instances of behaviour to determine equivalence of states to be merged based on statistical evidence. To avoid over-generalisation in the absence of labelled data, the EDSM algorithm was improved to incorporate inherent temporal behaviour (Walkinshaw et al. 2007; Walkinshaw and Bogdanov 2008), which needs to be known a priori. These approaches, however, do not always produce the most succinct automaton but generate an approximation that conforms to the trace (Ulyantsev, Buzhinsky, and Shalyto 2018). The comparative succinctness of our inferred automaton allows DeepSynth to be applied to large high-dimensional problems, including Montezuma’s Revenge. A detailed comparison of these approaches can be found in Section A of the Appendix.

A number of approaches combine SAT with state-merge to generate minimal automata from traces (Ulyantsev and Tsarev 2011; Heule and Verwer 2013; Ulyantsev, Buzhinsky, and Shalyto 2018; Buzhinsky and Vyatkin 2017; Buzhinsky and Vyatkin 2017). A similar SAT based algorithm is employed in (Xu et al. 2020) to generate reward machines. Although this approach generates succinct automata that accurately capture a rewarding sequence of events, it is not ideal for hard exploration problems such as Montezuma’s Revenge where reaching a rewarding state, e.g. collecting the key, requires the agent to follow a sequence of non-rewarding steps that are difficult to discover via exploration. The automata learning algorithm we use is able to capture these non-rewarding sequences and leverage it to guide exploration towards the rewarding states.

Inferred automata have been also used to learn strategies for infinite two-person games where strategies are a function of previously visited states. The construction of *chain automata* for these games provides a means to implement memory-less strategies (Krishnan et al. 1995), though these chain automata have a disproportionately large number of states as compared to the size of the actual automaton the game is played on.

Further related work is *policy sketching* (Andreas, Klein, and Levine 2017), which learns feasible tasks first and then stitches them together to accomplish a complex task. The key difference to our work is that the method assumes policy sketches, i.e. temporal instructions, to be available to the agent. There is also recent work on learning underlying non-Markovian objectives when an optimal policy or human demonstration is available (Koul, Fern, and Greydanus 2019; Memarian et al. 2020).

The rest of this paper is organised as follows. We first review fundamental notation and concepts in Section 3 and Section 4. DeepSynth technical details are then presented in Section 5, where we illustrate our method with Montezuma’s Revenge as the running example. Finally, Section 6 evaluates DeepSynth performance in a set of numerical experiments including Montezuma’s Revenge.

3 Background on Reinforcement Learning

We consider a conventional RL setup, consisting of an agent interacting with an environment, which is modelled as an unknown general Markov Decision Process (MDP):

Definition 3.1 (General MDP) The tuple $\mathfrak{M} = (\mathcal{S}, \mathcal{A}, s_0, P, \Sigma, L)$ is a general MDP over a set of continuous states \mathcal{S} , where \mathcal{A} is a finite set of actions and $s_0 \in \mathcal{S}$ is the initial state. $P : \mathcal{B}(\mathcal{S}) \times \mathcal{S} \times \mathcal{A} \rightarrow [0, 1]$ is a Borel-measurable conditional transition kernel that assigns to any pair of state $s \in \mathcal{S}$ and action $a \in \mathcal{A}$ a probability measure $P(\cdot|s, a)$ on the Borel space $(\mathcal{S}, \mathcal{B}(\mathcal{S}))$, where $\mathcal{B}(\mathcal{S})$ is the Borel sigma-algebra on the state space (Bertsekas and Shreve 2004). Σ is called the vocabulary set and it is a finite set of atomic propositions. There exists a labelling function $L : \mathcal{S} \rightarrow 2^\Sigma$ that assigns to each state $s \in \mathcal{S}$ a set of atomic propositions $L(s) \in 2^\Sigma$.

Definition 3.2 (Path) In a general MDP \mathfrak{M} , an infinite path ρ starting at s_0 is an infinite sequence of state transitions $s_0 \xrightarrow{a_0} s_1 \xrightarrow{a_1} \dots$ such that every transition $s_i \xrightarrow{a_i} s_{i+1}$ is possible in \mathfrak{M} , i.e. s_{i+1} belongs to the smallest Borel set B such that $P(B|s_i, a_i) = 1$. Similarly, a finite path is a finite sequence of state transitions $\rho_n = s_0 \xrightarrow{a_0} s_1 \xrightarrow{a_1} \dots \xrightarrow{a_{n-1}} s_n$. The set of infinite paths is $(\mathcal{S} \times \mathcal{A})^\omega$ and the set of finite paths is $(\mathcal{S} \times \mathcal{A})^* \times \mathcal{S}$.

At each state $s \in \mathcal{S}$, an agent action is determined by a policy π , which is a mapping from states to a probability distribution over the actions. That is, $\pi : \mathcal{S} \rightarrow \mathcal{P}(\mathcal{A})$. Further, a random variable $R(s, a) \sim \mathcal{Y}(\cdot|s, a) \in \mathcal{P}(\mathbb{R})$ is defined over the MDP \mathfrak{M} , to represent the Markovian reward obtained when action a is taken in a given state s , where $\mathcal{P}(\mathbb{R})$ is the set of probability distributions on subsets of \mathbb{R} , and \mathcal{Y} is the reward distribution. Similarly, a non-Markovian reward $\widehat{R} : (\mathcal{S} \times \mathcal{A})^* \times \mathcal{S} \rightarrow \mathbb{R}$ is a mapping from the set of finite paths to real numbers and one possible realisation of R and \widehat{R} at time step n is denoted by r_n and \widehat{r}_n respectively.

Definition 3.3 (Expected Discounted Return) For a policy π on an MDP \mathfrak{M} , the expected discounted return for a Markovian reward R is defined as (Sutton and Barto 1998):

$$U^\pi(s) = \mathbb{E}^\pi \left[\sum_{n=0}^{\infty} \gamma^n r_n | s_0 = s \right], \quad (1)$$

where $\mathbb{E}^\pi[\cdot]$ denotes the expected value given that the agent follows policy π , $[0, 1]$ ($\gamma \in [0, 1]$ when episodic) is a discount factor.

The expected return is also known as the *value function* in the literature. For any state-action pair (s, a) we can also define an action-value function that assigns a quantitative measure $Q : \mathcal{S} \times \mathcal{A} \rightarrow \mathbb{R}$ as follows:

$$Q^\pi(s, a) = \mathbb{E}^\pi \left[\sum_{n=0}^{\infty} \gamma^n r_n | s_0 = s, a_0 = a \right]. \quad (2)$$

Q-Learning (QL) (Watkins and Dayan 1992) employs the action-value function and updates state-action pair values upon visitation, as shown in (3). QL is *off-policy*, which means that π has no effect on the convergence of the Q-function, as long as every state-action pair is visited infinitely many times. Thus, for simplicity, we may use Q only as

$$Q(s, a) \leftarrow Q(s, a) + \alpha [R(s, a) + \gamma \max_{a' \in \mathcal{A}} (Q(s', a')) - Q(s, a)], \quad (3)$$

where $0 < \alpha \leq 1$ is the learning rate, γ is the discount factor, and s' is the state reached after performing action a . The learning rate and discount factor in general can be state-dependant. Under mild assumptions, QL converges to a unique limit Q^* , as long as every state action pair is visited infinitely many times (Watkins and Dayan 1992). Once QL converges, an optimal policy can be distilled from the action-value function:

$$\pi^*(s) = \arg \max_{a \in \mathcal{A}} Q^*(s, a),$$

where π^* is the same optimal policy that can be alternatively generated with Bellman iterations (Bertsekas and Tsitsiklis 1996) if the MDP was fully known, maximising the expected return (1) at any given state. Thus, the main goal is to synthesise π^* when the MDP is essentially a black box. We denote a non-Markovian optimal policy by $\widehat{\pi}^*$ which optimises a memory-dependent Q-function \widehat{Q}^* .

In many problems, the MDP can have a continuous or large state space, and thus the recursion in (3) has to be approximated by parameterising Q using a parameter set θ^Q . The parameters are updated by minimizing the following loss function (Riedmiller 2005):

$$\mathcal{L}(\theta^Q) = \mathbb{E}_{s \sim pr^\beta} [(Q(s, a|\theta^Q) - y)^2], \quad (4)$$

where pr^β is the probability distribution of state visit over \mathcal{S} under an arbitrary stochastic policy β , and

$$y = R(s, a) + \gamma \max_{a'} Q(s', a'|\theta^Q).$$

The function Q can then be approximated via a deep neural network architecture where the parameter set θ^Q represents the weights of the neural network.

4 Background on Automata Synthesis

This section describes the algorithm used for automatic inference of unknown high-level sequential structures as automata. The automata synthesis algorithm extracts information from trace sequences over finite paths in order to construct a succinct automaton that represents the behaviour exemplified by these traces. This architecture is an instance of the general *synthesis from examples* approach (Gulwani 2012; Jeppu et al. 2020). It is a scalable method for learning finite-state automaton from trace data that produces abstract, concise models. Our synthesis method scales to long traces by employing a segmentation approach, achieving automata learning in close-to-polynomial runtime (Jeppu 2020). Experimental evidence indicates a linear growth in runtime for increasing trace length in the case of segmented trace inputs, as compared to exponential growth for non-segmented trace inputs. Our algorithm learns succinct models from traces without the additional information that is typically required by the state-merge algorithm (Biermann and Feldman 1972b).

The synthesis algorithm takes as input a trace sequence and generates an N -state automaton conforming to the trace input. Starting with $N = 1$, the algorithm systematically searches for the required automaton, incrementing N by 1 each time the search fails. This ensures that the smallest automaton conforming to the input trace is generated. The algorithm

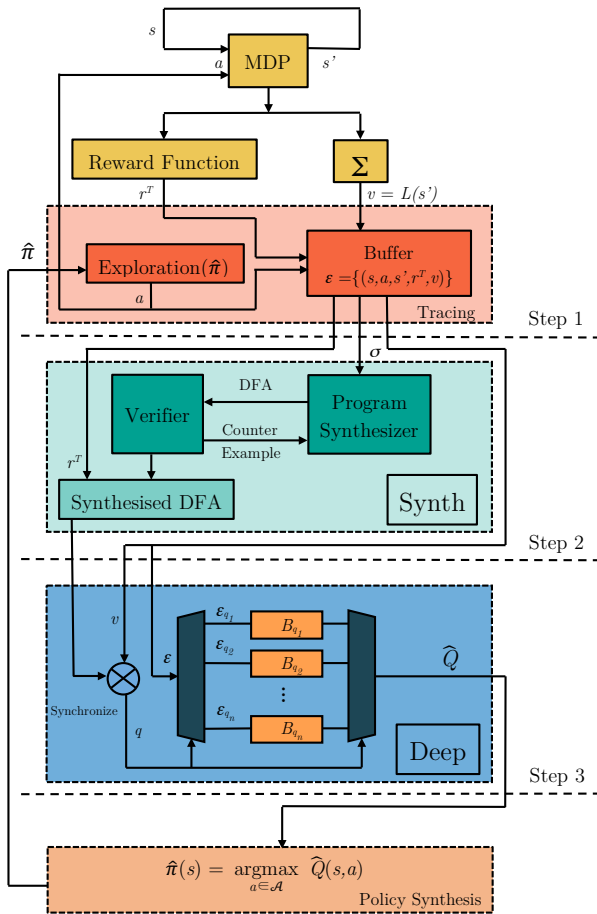


Figure 1: The DeepSynth Algorithm

additionally uses a hyper-parameter w to tackle growing algorithm complexity for long trace input. The synthesis algorithm divides the trace into segments using a sliding window of size w and only unique segments are used for further processing. In this way, the algorithm exploits the presence of patterns in traces. Multiple occurrences of these patterns are processed only once, thus reducing the size of the input to the algorithm.

Automata generated using only *positive* trace samples tend to overgeneralise (Gold 1978). This is mitigated by performing a compliance check of the automaton against the trace input to eliminate any transition sequences of length l that are accepted by the generated automaton but do not appear in the trace. The hyper-parameter l therefore controls the degree of generalisation in the generated automaton. A higher value for l yields more exact representations of the trace. The correctness of the generated automaton is verified by checking if the automaton accepts the input trace. If the check fails, missing trace data is incrementally added to refine the generated model, until the check passes. Further details on tuning the hyper-parameters w and l are given in the next section.

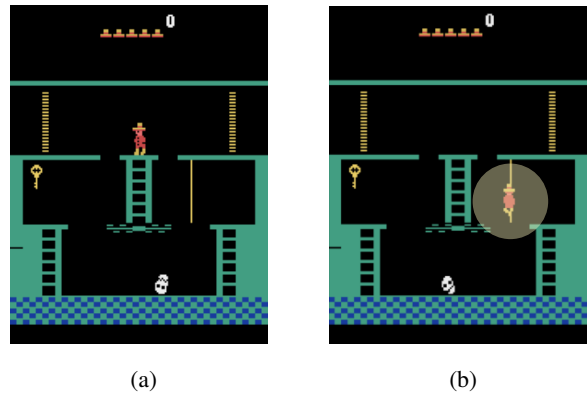


Figure 2: (a) the first level of Atari 2600 Montezuma's Revenge; (b) pixel overlap of two segmented objects.

5 DeepSynth

A schematic of the DeepSynth algorithm is provided in Fig. 1 and the algorithm is described step-by-step in this section. We begin by introducing the first level of Montezuma's Revenge as a running example (Bellemare et al. 2013). Unlike other Atari games where the primary goal is limited to avoiding obstacles or collecting items with no particular order, Montezuma's Revenge requires the agent to perform a long, complex sequence of actions before receiving any reward. The agent must find a key and open either door in Fig. 2.a. To this end, the agent has to climb down the middle ladder, jump on the rope, climb down the ladder on the right and jump over a skull to reach the key. The reward given by the Atari emulator for collecting the key is 100 and the reward for opening one of the doors is another 300. Owing to the sparsity of the rewards the existing deep RL algorithms either fail to learn a policy that can even reach the key, e.g. DQN (Mnih et al. 2015), or the learning process is computationally heavy and sample inefficient, e.g. FeUdal (Vezhnevets et al. 2017), and Go-Explore (Ecoffet et al. 2021).

Existing techniques to solve this problem mostly hinge on intrinsic motivation and object-driven guidance. Unsupervised object detection (or unsupervised semantic segmentation) from raw image input has seen substantial progress in recent years, and became comparable to its supervised counterpart (Liu et al. 2019; Ji, Henriques, and Vedaldi 2019; Hwang et al. 2019; Zheng and Yang 2021). In this work, we assume that an off-the-shelf image segmentation algorithm can provide plausible object candidates, e.g. (Liu et al. 2019). The key to solving a complex task such as Montezuma's Revenge is finding the semantic correlation between the objects in the scene. When a human player tries to solve this game the semantic correlations, such as "keys open doors", are partially known and the player's behaviour is driven by exploiting these known correlations when exploring unknown objects. This drive to explore unknown objects has been a subject of study in psychology, where animals and humans seem to have general motivations (often referred to as intrinsic motivations) that push them to explore and manipulate their environment, encouraging curiosity and cognitive

growth (Berlyne 1960; Csikszentmihalyi 1990; Ryan and Deci 2000).

As explained later, DeepSynth encodes these correlations as an automaton, which is an intuitive and modular structure, and guides the exploration so that previously unknown correlations are discovered. This exploration scheme imitates biological cognitive growth in a formal and explainable way, and is driven by an intrinsic motivation to explore as many objects as possible in order to find the optimal sequence of extrinsically-rewarding high-level objectives. To showcase the full potential of DeepSynth, in all the experiments and examples of this paper we assume that semantic correlations are unknown to the agent. The agent starts with no prior knowledge of the sparse reward task or the correlation of the high-level objects.

Let us write Σ for the set of detected objects. Note that the semantics of the names for individual objects is of no relevance to the algorithm and Σ can thus contain any distinct identifiers, e.g. $\Sigma = \{\text{obj}_1, \text{obj}_2, \dots\}$. But for the sake of exposition we name the objects according to their appearance in Fig. 2.a, i.e. $\Sigma = \{\text{red_character}, \text{middle_ladder}, \text{rope}, \text{right_ladder}, \text{left_ladder}, \text{key}, \text{door}\}$. Note that there can be any number of detected objects, as long as the input image is segmented into enough objects whose correlation can guide the agent to achieve the task.

Tracing (Step 1 in Fig. 1)

Note that the task is unknown initially and the extrinsic reward is non-Markovian and extremely sparse. The agent receives a reward $\widehat{R} : (\mathcal{S} \times \mathcal{A})^* \times \mathcal{S} \rightarrow \mathbb{R}$ only when a correct sequence of state-action pairs and their associated object correlations are visited. In order to guide the agent to find the optimal sequence, DeepSynth uses the following reward transformation:

$$r^T = \widehat{r} + \mu r^i, \quad (5)$$

where \widehat{r} is the extrinsic reward, $\mu > 0$ is a positive regulatory coefficient, and r^i is the intrinsic reward. The role of the intrinsic reward is to guide the exploration and also to drive the exploration towards the discovery of unknown object correlations. The underlying mechanism of intrinsic rewards depends on the inferred automaton and is explained in detail later. The only extrinsic rewards in Montezuma’s Revenge are the reward for reaching the key \widehat{r}_{key} and for reaching one of the doors \widehat{r}_{door} . Note that the lack of intrinsic motivation as shown in Section 6, prevents other methods, e.g. (Toro Icarte et al. 2019; Rens et al. 2020; Gaon and Brafman 2020; Xu et al. 2020), to succeed in extremely-sparse reward, high-dimensional and large problems such as Montezuma’s Revenge. DeepSynth pseudo-code is in the Appendix.

In Montezuma’s Revenge, states consist of raw pixel images. Each state is a stack of four consecutive frames $84 \times 84 \times 4$ that are preprocessed to reduce input dimensionality (Mnih et al. 2015). The labelling function employs the object vocabulary set Σ to detect object pixel overlap in a particular state frame. For example, if the pixels of `red_character` collide with the pixels of `rope` in any of the stacked frames, the labelling function for that particular

state s is $L(s) = \{\text{red_character}, \text{rope}\}$ (Fig. 2.b). In this specific example, the only moving object is the character. So for sake of succinctness, we omit the character from the label set, e.g., the above label is $L(s) = \{\text{rope}\}$.

Given this labelling function, Tracing (Step 1) records the sequence of detected objects $L(s_i)L(s_{i+1}) \dots$ as the agent explores the MDP. The labelling function, as per Definition 3.1, is a mapping from the state space to the power set of objects in the vocabulary $L : \mathcal{S} \rightarrow 2^\Sigma$ and thus, the label of a state could be the empty set or a set of objects.

All transitions with their corresponding labels are stored as 5-tuples $\langle s, a, s', r^T, L(s') \rangle$, where s is the current state, a is the executed action, s' is the resulting state, r^T is the total reward received after performing action a at state s , and $L(s')$ is the label corresponding to the set of atomic propositions in Σ that hold in state s' . The set of past experiences is called the experience replay buffer \mathcal{E} . The exploration process generates a set of *traces*, defined as follows:

Definition 5.1 (Trace) *In a general MDP \mathfrak{M} , and over a finite path $\rho_n = s_0 \xrightarrow{a_0} s_1 \xrightarrow{a_1} \dots \xrightarrow{a_{n-1}} s_n$, a trace σ is defined as a sequence of labels $\sigma = v_1, v_2, \dots, v_n$, where $v_i = L(s_i)$ is a trace event.*

The set of traces associated with \mathcal{E} is denoted by \mathcal{T} . The tracing scheme is the Tracing box in Fig. 1.

Synth (Step 2 in Fig. 1)

The automata synthesis algorithm described in Section 4 is used to generate an automaton that conforms to the trace sequences generated by Tracing (Step 1). Given a trace sequence $\sigma = v_1, v_2, \dots, v_n$, the labels v_i serve as transition predicates in the generated automaton. The synthesis algorithm further constrains the construction of the automaton so that no two transitions from a given state in the generated automaton have the same predicates. The automaton obtained by the synthesis algorithm is thus deterministic. The learned automaton follows the standard definition of a Deterministic Finite Automaton (DFA) with the alphabet $\Sigma_{\mathfrak{A}}$, where a symbol of the alphabet $v \in \Sigma_{\mathfrak{A}}$ is given by the labelling function $L : \mathcal{S} \rightarrow 2^\Sigma$ defined earlier. Thus, given a trace sequence $\sigma = v_1, v_2, \dots, v_n$ over a finite path $\rho_n = s_0 \xrightarrow{a_0} s_1 \xrightarrow{a_1} \dots \xrightarrow{a_{n-1}} s_n$ in the MDP, the symbol $v_i \in \Sigma_{\mathfrak{A}}$ is given by $v_i = L(s_i)$.

The Atari emulator provides the number of lives left in the game, which is used to reset $\Sigma_{\mathfrak{A}} \subseteq \Sigma_{\mathfrak{A}}$, where $\Sigma_{\mathfrak{A}}$ is the set of labels that appeared in the trace so far. Upon losing a life, $\Sigma_{\mathfrak{A}}$ is reset to the empty set.

Definition 5.2 (Deterministic Finite Automaton) *A DFA $\mathfrak{A} = (\mathcal{Q}, q_0, \Sigma_{\mathfrak{A}}, F, \delta)$ is a 5-tuple, where \mathcal{Q} is a finite set of states, $q_0 \in \mathcal{Q}$ is the initial state, $\Sigma_{\mathfrak{A}}$ is the alphabet, $F \subset \mathcal{Q}$ is the set of accepting states, and $\delta : \mathcal{Q} \times \Sigma_{\mathfrak{A}} \rightarrow \mathcal{Q}$ is the transition function.*

Let $\Sigma_{\mathfrak{A}}^*$ be the set of all finite words over $\Sigma_{\mathfrak{A}}$. A finite word $w = v_1, v_2, \dots, v_m \in \Sigma_{\mathfrak{A}}^*$ is accepted by a DFA \mathfrak{A} if there exists a finite run $\theta \in \mathcal{Q}^*$ starting from $\theta_0 = q_0$, where $\theta_{i+1} = \delta(\theta_i, v_{i+1})$ for $i \geq 0$ and $\theta_m \in F$. Given the collected traces \mathcal{T} we construct a DFA using the method described in Section 4. The algorithm first divides the trace

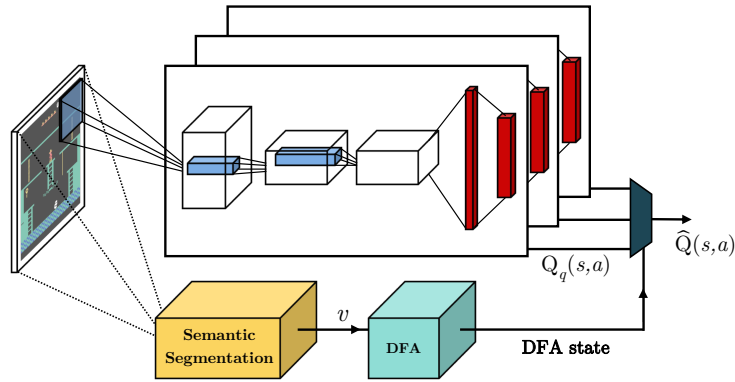


Figure 3: DeepSynth for Montezuma’s Revenge: each DQN module is forced by the DFA to focus on the correlation of semantically distinct objects.

into segments using a sliding window of size equal to the hyper-parameter w introduced earlier. This determines the size of the input to the search procedure, and consequently the algorithm runtime. Note that choosing $w = 1$ will not capture any sequential behaviour. In DeepSynth, we would like to have a value for w that results in the smallest input size. In our experiments, we tried different values for w in increasing order, ranging within $1 < w \leq |\sigma|$, and have obtained the same automaton in all setups.

As discussed in Section 4, the hyper-parameter l controls the degree of generalisation in the learnt automaton. Learning exact automata from trace data is known to be NP-complete (Gold 1978). Thus, a higher value for l increases the algorithm runtime. We optimise over the hyper-parameters and choose $w = 3$ and $l = 2$ as the best fit for our setting. This ensures that the automata synthesis problem is not too complex for the synthesis algorithm to solve but at the same time it does not over-generalise to fit the trace.

The generated automaton provides deep insight into the correlation of the objects detected in Step 1 and shapes the intrinsic reward. The output of this stage is a DFA, from the set of succinct DFAs obtained earlier. Fig. 4 gives three exemplars of the evolution of the synthesised automata for Montezuma’s Revenge. Most of the deep RL approaches are able to reach the states that correspond to the DFA in Fig. 4.a via random exploration. However, reaching the key and further the doors as in Fig. 4.b and Fig. 4.c is challenging and is achieved by DeepSynth using a hierarchical curiosity-driven learning method described next. The automata synthesis is the Synth box in Fig. 1 and implementation details can be found in (Hasanbeig et al. 2019b).

Deep Temporal Neural Fitted RL (Step 3 in Fig. 1)

We propose a deep-RL-based architecture inspired by DQN (Mnih et al. 2015) and Neural Fitted Q -iteration (NFQ) (Riedmiller 2005) when the input is in vector form, not a raw image. DeepSynth is able to synthesise a policy whose traces are accepted by the DFA and it encourages the agent to explore under the DFA guidance. More importantly, the

agent is guided and encouraged to expand the DFA towards task satisfaction.

Given the constructed DFA, at each time step during the learning episode, if a new label is observed during exploration, the intrinsic reward in (5) becomes positive. Namely,

$$R^i(s, a) = \begin{cases} \eta & \text{if } L(s') \notin \Sigma_a, \\ 0 & \text{otherwise,} \end{cases} \quad (6)$$

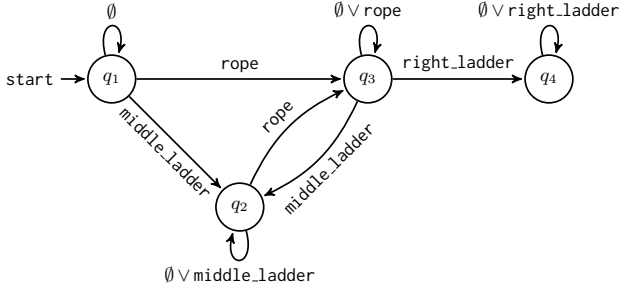
where η is an arbitrarily finite and positive reward, and Σ_a , as discussed in the Synth step, is the set of labels that the agent has observed *in the current learning episode*. Further, once a new label that does not belong to Σ_a is observed during exploration (Step 1) it is then passed to the automaton synthesis step (Step 2). The automaton synthesis algorithm then synthesises a new DFA that complies with the new label.

For example, in Montezuma’s revenge, the agent will get intrinsic reward every time it reaches the middle ladder for the first time during a trace, not just on the first trace it reaches that ladder. Furthermore, note that the intrinsic reward is used to motivate exploration and to discover new label objects. The overall task is initially unknown, thus *bad* high-level actions cannot be inferred solely from the labels. Note that whenever the agent is intrinsically rewarded towards a bad behaviour, the contribution from the extrinsic reward is much higher than that from the intrinsic reward (adjusted by μ in (6)). Thus, the agent is able to escape local intrinsic optima and backpropagate the extrinsic reward to rule out bad behaviours and find the extrinsic optimal policy. In principle, if a high-level objective could be labelled as *bad*, namely if the task is partially known, then the intrinsic reward could as well account for that.

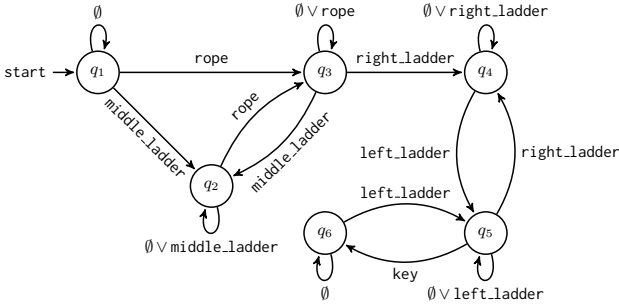
Theorem 5.1 (Formalisation of the Intrinsic Reward)

The optimal policies are invariant under the reward transformation in (5) and (6).

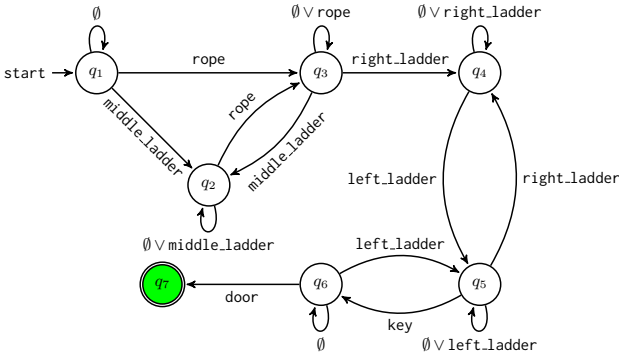
Proof. We leverage the concept of reward shaping to prove that the generated policies under the intrinsic reward transformation are guaranteed to be optimal with respect to the original extrinsic reward function (Ng, Harada, and Russell



(a) The right ladder is often discovered by random exploration



(b) The key is found with an extrinsic reward of $\hat{r}_{key} = +100$



(c) The door is unlocked with an extrinsic reward of $\hat{r}_{door} = +300$

Figure 4: Illustration of the evolution of the automaton synthesised for Montezuma’s Revenge. Note that the agent found a short-cut to reach the key by skipping the middle ladder and directly jumping over the rope, which is not obvious even to a human player. Such observations are difficult to extract from other hierarchy representations, e.g. LSTMs.

1999; Grześ 2017). (Ng, Harada, and Russell 1999) proved that given any MDP $\mathfrak{M} = (\mathcal{S}, \mathcal{A}, s_0, P, \Sigma, L)$, if there exists a potential function $\Phi : \mathcal{S} \rightarrow \mathbb{R}$, such that it transforms the reward function r of MDP \mathfrak{M} to

$$r'(s, a, s') = r(s, a, s') + \gamma\Phi(s') - \Phi(s),$$

then the set of optimal policies are invariant under r' . We define the potential function as

$$\Phi(s) = \begin{cases} \mu(\eta/\gamma) & \text{if } L(s) \notin \Sigma_a, \\ 0 & \text{otherwise.} \end{cases} \quad (7)$$

Note that the potential function is bounded, and (5) can be formalised as a formal reward shaping, in which the intrinsic reward r^i is proved not to be part of the original optimisation problem. \square

In the following, in order to explain the core ideas underpinning the algorithm, we temporarily assume that the MDP graph and the associated transition probabilities are fully known. Later we relax these assumptions, and we stress that the algorithm can be run *model-free* over any black-box MDP environment. Specifically, we relate the black-box MDP and the automaton by synchronising them *on-the-fly* to create a new structure that breaks down a non-Markovian task into a set of Markovian, history-independent sub-goals.

Definition 5.3 (Product MDP) Given an MDP $\mathfrak{M} = (\mathcal{S}, \mathcal{A}, s_0, P, \Sigma)$ and a DFA $\mathfrak{A} = (\mathcal{Q}, q_0, \Sigma_{\mathfrak{A}}, F, \delta)$, the product MDP is defined as $(\mathfrak{M} \otimes \mathfrak{A}) = \mathfrak{M}_{\mathfrak{A}} = (\mathcal{S}^{\otimes}, \mathcal{A}, s_0^{\otimes}, P^{\otimes}, \Sigma^{\otimes}, F^{\otimes})$, where $\mathcal{S}^{\otimes} = \mathcal{S} \times \mathcal{Q}$, $s_0^{\otimes} = (s_0, q_0)$, $\Sigma^{\otimes} = \mathcal{Q}$, and $F^{\otimes} = \mathcal{S} \times F$. The transition kernel P^{\otimes} is such that given the current state (s_i, q_i) and action a , the new state (s_j, q_j) is given by $s_j \sim P(\cdot | s_i, a)$ and $q_j = \delta(q_i, L(s_j))$.

By synchronising MDP states with the DFA states by means of the product MDP, we can evaluate the satisfaction of the associated high-level task. Most importantly, as shown in (Brafman, De Giacomo, and Patrizi 2018), for any MDP \mathfrak{M} with finite-horizon non-Markovian reward, e.g. Montezuma’s Revenge, there exists a Markov reward MDP $\mathfrak{M}' = (\mathcal{S}, \mathcal{A}, s_0, P, \Sigma)$ that is equivalent to \mathfrak{M} such that the states of \mathfrak{M} can be mapped into those of \mathfrak{M}' . The corresponding states yield the same transition probabilities, and corresponding traces have the same rewards. Based on this result, (De Giacomo et al. 2019) showed that the product MDP $\mathfrak{M}_{\mathfrak{A}}$ is \mathfrak{M}' defined above. Therefore, the non-Markovianity of the extrinsic reward is resolved by synchronising the DFA with the original MDP, where the DFA represents the history of state labels that has led to that reward.

Note that the DFA transitions can be executed just by observing the labels of the visited states, which makes the agent aware of the automaton state without explicitly constructing the product MDP. This means that the proposed approach can run *model-free*, and as such it does not require a priori knowledge about the MDP.

Each state of the DFA in the synchronised product MDP divides the general sequential task so that each transition between the states represents an achievable Markovian sub-task. Thus, given a synthesised DFA $\mathfrak{A} = (\mathcal{Q}, q_0, \Sigma_{\mathfrak{A}}, F, \delta)$, we propose a hybrid architecture of $n = |\mathcal{Q}|$ separate deep RL modules (Fig. 3 and Deep in Fig. 1). For each state in the DFA, there is a dedicated deep RL module, where each deep RL module is an instance of a deep RL algorithm with distinct neural networks and replay buffers. The modules are interconnected, in the sense that modules act as a global *hybrid* deep RL architecture to approximate the Q -function in the product MDP. As explained in the following, this allows the agent to jump from one sub-task to another by just switching between these modules as prescribed by the DFA.

In the running example, the agent exploration scheme is ϵ -greedy with diminishing ϵ where the rate of decrease also depends on the DFA state so that each module has enough

chance to explore. For each automaton state $q_i \in \mathcal{Q}$ in the the product MDP, the associated deep RL module is called $B_{q_i}(s, a)$. Once the agent is at state $s^{\otimes} = (s, q_i)$, the neural net B_{q_i} is active and explores the MDP. Note that the modules are interconnected, as discussed above. For example, assume that by taking action a in state $s^{\otimes} = (s, q_i)$ the label $v = L(s')$ has been observed and as a result the agent is moved to state $s^{\otimes'} = (s', q_j)$, where $q_i \neq q_j$. By minimising the loss function \mathcal{L} the weights of B_{q_i} are updated such that $B_{q_i}(s, a)$ has minimum possible error to $R^T(s, a) + \gamma \max_{a'} B_{q_j}(s', a')$ while $B_{q_i} \neq B_{q_j}$. As such, the output of B_{q_j} directly affects B_{q_i} when the automaton state is changed. This allows the extrinsic reward to back-propagate efficiently, e.g. from modules B_{q_7} and B_{q_6} associated with q_7 and q_6 in Fig. 4.c, to the initial module B_{q_1} .

Define \mathcal{E}_{q_i} as the projection of the general replay buffer \mathcal{E} onto q_i . The size of the replay buffer for each module is limited and in the case of our running example $|\mathcal{E}_{q_i}| = 15000$. This includes the most recent frames that are observed when the product MDP state was $s^{\otimes} = (s, q_i)$. In the running example we used RMSProp for each module with uniformly sampled mini-batches of size 32. When the state is in vector form and no convolutional layer is involved we resort to NFQ deep RL modules instead of DQN modules.

6 Experimental Results

Benchmarks and Setup

We evaluate and compare the performance of DeepSynth with DQN on a comprehensive set of benchmarks, given in Table 1. The Minecraft environment (`minecraft-tx`) taken from (Andreas, Klein, and Levine 2017) requires solving challenging low-level control tasks, and features highly sequential high-level goals. The two `mars-rover` benchmarks are taken from (Hasanbeig, Abate, and Kroening 2019b), and the models have uncountably infinite state spaces. The example `robot-surve` is adopted from (Sadigh et al. 2014), and the task is to visit two regions in sequence. Models `s1p-easy` and `s1p-hard` are inspired by the noisy MDPs of Chapter 6 in (Sutton and Barto 1998). The goal in `s1p-easy` is to reach a particular region of the MDP and the goal in `s1p-hard` is to visit four distinct regions sequentially in proper order. The `frozen-lake` benchmarks are similar: the first three are simple reachability problems and the last three require sequential visits of four regions, except that now there exist unsafe regions as well. The `frozen-lake` MDPs are stochastic and are adopted from the OpenAI Gym (Brockman et al. 2016).

The *task DFA* column in Table 1 gives the number of states in the automaton that can be generated from the high-level objective sequences of the ground-truth task. The *synth DFA* column gives the number of states of the automaton synthesised by DeepSynth, and *prod. MDP* gives the number of states in the resulting product MDP (Definition 5.3). Finally, *max sat. prob. at s_0* is the maximum probability of achieving the extrinsic reward from the initial state. In all experiments the high-level objective sequences are initially unknown to the agent. Furthermore, the extrinsic reward is only given when completing the task and reaching the objectives in the

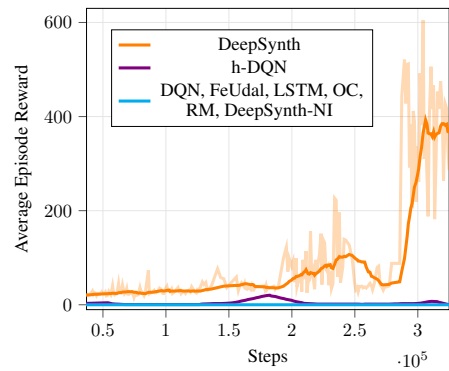


Figure 5: Average episode reward progress in Montezuma’s Revenge with h-DQN (Kulkarni et al. 2016), DQN (Mnih et al. 2015), FeUdal-LSTM (Vezhnevets et al. 2017), Option-Critic (OC) (Bacon, Harb, and Precup 2017), inferring reward models (RM) (Toro Icarte et al. 2019; Rens et al. 2020; Gaon and Brafman 2020; Xu et al. 2020) and DeepSynth with no intrinsic reward (DeepSynth-NI). h-DQN (Kulkarni et al. 2016) finds the door but only after 2M steps. FeUdal and LSTM find the door after 100M and 200M steps respectively. DQN, OC, RM and DeepSynth-NI remain flat.

correct order. The details of all experiments, including hyper-parameters, are given in the Appendix.

Results

The training progress for Montezuma’s Revenge and Task 3 in Minecraft is plotted in Fig. 5 and Fig. 6. In Fig. 6.a the orange line gives the loss for the very first deep net associated to the initial state of the DFA, the red and blue ones are of the intermediate states in the DFA and the green line is associated to the final state. This shows an efficient back-propagation of extrinsic reward from the final high-level state to the initial state, namely once the last deep net converges the expected reward is back-propagated to the second and so on. Each NFQ module has 2 hidden layers and 128 ReLUs. Note that there may be a number of ways to accomplish a particular task in the synthesised DFAs. This, however, causes no harm since when the extrinsic reward is back-propagated, the non-optimal options fall out. Further, emphasise that if the task DFA, in any of the experiments, is known or even partially known a priori, then the Synth step can exploit this partial automaton by incrementally adding any new labels or subtask sequences discovered during exploration. As an example, if the automaton in Fig. 4.b is given initially, the agent is able to utilise the semantic correlation of the objects to facilitate its explorations and find the key faster.

7 Conclusions

We have proposed a fully-unsupervised approach for training deep RL agents when the reward is extremely sparse and non-Markovian. We *automatically* infer a high-level structure from observed exploration traces using automata synthesis. The inferred automaton is a formal, un-grounded, human-interpretable representation of a complex task and its steps.

experiment	$ S $	task DFA	synth DFA	prod. MDP	max sat. prob. at s_0	DeepSynth conv. ep.*	DQN conv. ep.*
minecraft-t1	100	3	6	600	1	25	40
minecraft-t2	100	3	6	600	1	30	45
minecraft-t3	100	5	5	500	1	40	t/o
minecraft-t4	100	3	3	300	1	30	50
minecraft-t5	100	3	6	600	1	20	35
minecraft-t6	100	4	5	500	1	40	t/o
minecraft-t7	100	5	7	800	1	70	t/o
mars-rover-1	∞	3	3	∞	n/a	40	50
mars-rover-2	∞	4	4	∞	n/a	40	t/o
robot-surve	25	3	3	75	1	10	10
slp-easy-sm1	120	2	2	240	1	10	10
slp-easy-med	400	2	2	800	1	20	20
slp-easy-lrg	1600	2	2	3200	1	30	30
slp-hard-sm1	120	5	5	600	1	80	t/o
slp-hard-med	400	5	5	2000	1	100	t/o
slp-hard-lrg	1600	5	5	8000	1	120	t/o
frozen-lake-1	120	3	3	360	0.9983	100	120
frozen-lake-2	400	3	3	1200	0.9982	150	150
frozen-lake-3	1600	3	3	4800	0.9720	150	150
frozen-lake-4	120	6	6	720	0.9728	300	t/o
frozen-lake-5	400	6	6	2400	0.9722	400	t/o
frozen-lake-6	1600	6	6	9600	0.9467	450	t/o

* average number of episodes to convergence over 10 runs

Table 1: Comparison between DeepSynth and DQN

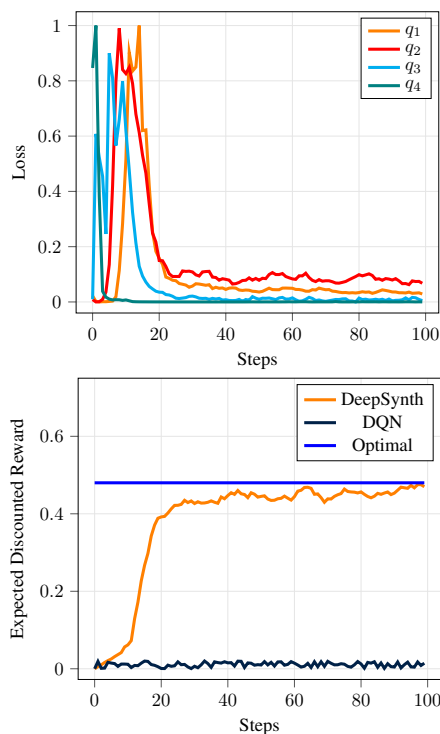


Figure 6: Minecraft Task 3 Experiment: (a) Training progress with four hybrid deep NFQ modules, (b) Training progress with DeepSynth and DQN on the same training set \mathcal{E} .

We showed that we are able to efficiently learn policies that achieve complex high-level objectives using fewer training samples as compared to alternative algorithms. Owing to the modular structure of the automaton, the overall task can be segmented into easy Markovian sub-tasks. Therefore, any segment of the proposed network that is associated with a sub-task can be used as a separate trained module in transfer learning. Another major contribution of the proposed method is that in problems where domain knowledge is available, this knowledge can be easily encoded as an automaton to guide learning. This enables the agent to solve complex tasks and saves the agent from an exhaustive exploration in the beginning.

References

- Abbeel, P.; Coates, A.; Quigley, M.; and Ng, A. Y. 2007. An Application of Reinforcement Learning to Aerobatic Helicopter Flight. In *NeurIPS*, 1–8. MIT Press.
- Andreas, J.; Klein, D.; and Levine, S. 2017. Modular Multi-task Reinforcement Learning with Policy Sketches. In *ICML*, volume 70, 166–175.
- Angluin, D. 1987. Learning Regular Sets from Queries and Counterexamples. *Inf. Comput.* 75(2): 87–106.
- Bacon, P.-L.; Harb, J.; and Precup, D. 2017. The Option-critic Architecture. In *AAAI*.
- Bellemare, M. G.; Naddaf, Y.; Veness, J.; and Bowling, M. 2013. The Arcade Learning Environment: An Evaluation Platform for General Agents. *Artificial Intelligence Research* 47: 253–279.
- Berlyne, D. E. 1960. *Conflict, Arousal, and Curiosity*. McGraw-Hill Book Company.
- Bertsekas, D. P.; and Shreve, S. 2004. *Stochastic Optimal Control: The Discrete-time Case*. Athena Scientific.
- Bertsekas, D. P.; and Tsitsiklis, J. N. 1996. *Neuro-dynamic Programming*, volume 1. Athena Scientific.
- Biermann, A. W.; and Feldman, J. A. 1972a. On the Synthesis of Finite-State Machines from Samples of Their Behavior. *IEEE Trans. Comput.* 21(6): 592–597.
- Biermann, A. W.; and Feldman, J. A. 1972b. On the Synthesis of Finite-State Machines from Samples of Their Behavior. *IEEE Trans. Comput.* 21(6): 592–597.
- Brafman, R. I.; De Giacomo, G.; and Patrizi, F. 2018. LTLf/LDLf Non-Markovian Rewards. In *AAAI*.
- Brockman, G.; Cheung, V.; Pettersson, L.; Schneider, J.; Schulman, J.; Tang, J.; and Zaremba, W. 2016. OpenAI Gym. *arXiv* 1606.01540.
- Buzhinsky, I.; and Vyatkin, V. 2017. Automatic Inference of Finite-State Plant Models From Traces and Temporal Properties. *IEEE Trans. Ind. Informat.* 13(4): 1521–1530.
- Buzhinsky, I.; and Vyatkin, V. 2017. Modular Plant Model Synthesis from Behavior Traces and Temporal Properties. In *Emerging Technologies and Factory Automation*, 1–7. IEEE.
- Cai, M.; Peng, H.; Li, Z.; Gao, H.; and Kan, Z. 2021. Receding Horizon Control-Based Motion Planning With Partially Infeasible LTL Constraints. *IEEE Control Systems Letters* 5(4): 1279–1284.
- Camacho, A.; Toro Icarte, R.; Klassen, T. Q.; Valenzano, R.; and McIlraith, S. A. 2019. LTL and Beyond: Formal Languages for Reward Function Specification in Reinforcement Learning. In *IJCAI*, 6065–6073.
- Chockler, H.; Kesseli, P.; Kroening, D.; and Strichman, O. 2020. Learning the Language of Software Errors. *Artificial Intelligence Research* 67: 881–903.
- Cook, S.; and Mitchell, D. 1996. Finding Hard Instances of the Satisfiability Problem: A Survey. In *Satisfiability Problem: Theory and Applications*.
- Csikszentmihalyi, M. 1990. *Flow: The Psychology of Optimal Experience*. Harper & Row New York.
- Daniel, C.; Neumann, G.; and Peters, J. 2012. Hierarchical relative entropy policy search. In *Artificial Intelligence and Statistics*, 273–281.
- Davis, M.; and Putnam, H. 1960. A Computing Procedure for Quantification Theory. *J. ACM* 7(3): 201–215.
- De Giacomo, G.; Favorito, M.; Iocchi, L.; and Patrizi, F. 2020. Imitation Learning over Heterogeneous Agents with Restraining Bolts. In *International Conference on Automated Planning and Scheduling*, 517–521.
- De Giacomo, G.; Iocchi, L.; Favorito, M.; and Patrizi, F. 2019. Foundations for Restraining Bolts: Reinforcement Learning with LTLf/LDLf Restraining Specifications. In *International Conference on Automated Planning and Scheduling*, volume 29, 128–136.
- Ecoffet, A.; Huizinga, J.; Lehman, J.; Stanley, K. O.; and Clune, J. 2021. First Return, Then Explore. *Nature* 590(7847): 580–586.
- Fu, J.; and Topcu, U. 2014. Probably Approximately Correct MDP Learning and Control With Temporal Logic Constraints. In *Robotics: Science and Systems X*.
- Fulton, N.; and Platzer, A. 2018. Safe Reinforcement Learning via Formal Methods: Toward Safe Control Through Proof and Learning. In *AAAI*, 6485–6492.
- Furelos-Blanco, D.; Law, M.; Russo, A.; Broda, K.; and Jonsson, A. 2020. Induction of Subgoal Automata for Reinforcement Learning. In *AAAI*, 3890–3897.
- Gaon, M.; and Brafman, R. 2020. Reinforcement Learning with Non-Markovian Rewards. In *Proceedings of the AAAI Conference on Artificial Intelligence*, volume 34, 3980–3987.
- Glover, F.; and Laguna, M. 1998. Tabu Search. In *Handbook of Combinatorial Optimization*, volume 1–3, 2093–2229. Springer.
- Gold, E. M. 1978. Complexity of Automaton Identification from Given Data. *Information and Control* 37: 302–320.
- Grześ, M. 2017. Reward Shaping in Episodic Reinforcement Learning. In *Autonomous Agents and Multiagent Systems*, 565–573. International Foundation for Autonomous Agents and Multiagent Systems.
- Gulwani, S. 2012. Synthesis from Examples. In *WAMBSE*.
- Hahn, E. M.; Perez, M.; Schewe, S.; Somenzi, F.; Trivedi, A.; and Wojtczak, D. 2019. Omega-Regular Objectives in Model-Free Reinforcement Learning. In *TACAS*, 395–412. Springer.
- Hasanbeig, M.; Abate, A.; and Kroening, D. 2018. Logically-Constrained Reinforcement Learning. *arXiv* 1801.08099.
- Hasanbeig, M.; Abate, A.; and Kroening, D. 2019a. Certified Reinforcement Learning with Logic Guidance. *arXiv* 1902.00778.
- Hasanbeig, M.; Abate, A.; and Kroening, D. 2019b. Logically-Constrained Neural Fitted Q-Iteration. In *Autonomous Agents and Multiagent Systems*, 2012–2014. Inter-

- national Foundation for Autonomous Agents and Multiagent Systems.
- Hasanbeig, M.; Abate, A.; and Kroening, D. 2020. Cautious Reinforcement Learning with Logical Constraints. In *Autonomous Agents and Multiagent Systems*, 483–491. International Foundation for Autonomous Agents and Multiagent Systems.
- Hasanbeig, M.; Kantaros, Y.; Abate, A.; Kroening, D.; Pappas, G. J.; and Lee, I. 2019a. Reinforcement Learning for Temporal Logic Control Synthesis with Probabilistic Satisfaction Guarantees. In *CDC*, 5338–5343. IEEE.
- Hasanbeig, M.; Kroening, D.; and Abate, A. 2020. Deep Reinforcement Learning with Temporal Logics. In *Formal Modeling and Analysis of Timed Systems*, volume 12288 of *LNCS*, 1–22. Springer.
- Hasanbeig, M.; Yogananda Jeppu, N.; Abate, A.; Melham, T.; and Kroening, D. 2019b. DeepSynth: Program Synthesis for Automatic Task Segmentation in Deep Reinforcement Learning [Extended Version]. *arXiv* 1911.10244.
- Heule, M. J. H.; and Verwer, S. 2013. Software Model Synthesis Using Satisfiability Solvers. *Empirical Software Engineering* 18(4): 825–856.
- Hwang, J.-J.; Yu, S. X.; Shi, J.; Collins, M. D.; Yang, T.-J.; Zhang, X.; and Chen, L.-C. 2019. SegSort: Segmentation by Discriminative Sorting of Segments. In *ICCV*, 7334–7344.
- Jeppu, N. Y. 2020. *Trace2Model Github repository*. URL <https://github.com/natasha-jeppu/Trace2Model>.
- Jeppu, N. Y.; Melham, T.; Kroening, D.; and O’Leary, J. 2020. Learning Concise Models from Long Execution Traces. In *Design Automation Conference*, 1–6. ACM/IEEE.
- Ji, X.; Henriques, J. F.; and Vedaldi, A. 2019. Invariant Information Clustering for Unsupervised Image Classification and Segmentation. In *ICCV*, 9865–9874.
- Kazemi, M.; and Soudjani, S. 2020. Formal Policy Synthesis for Continuous-Space Systems via Reinforcement Learning. *arXiv* 2005.01319.
- Kearns, M.; and Singh, S. 2002. Near-optimal Reinforcement Learning in Polynomial Time. *Machine Learning* 49(2-3): 209–232.
- Kingma, D. P.; and Ba, J. 2015. Adam: A Method for Stochastic Optimization. In *International Conference on Learning Representations*.
- Koul, A.; Fern, A.; and Greydanus, S. 2019. Learning Finite State Representations of Recurrent Policy Networks. In *International Conference on Learning Representations*.
- Krishnan, S. C.; Puri, A.; Brayton, R. K.; and Varaiya, P. P. 1995. The Rabin Index and Chain Automata, with Applications to Automata and Games. In *Computer-Aided Verification (CAV)*, *LNCS*, 253–266. Springer.
- Kulkarni, T. D.; Narasimhan, K.; Saeedi, A.; and Tenenbaum, J. 2016. Hierarchical Deep Reinforcement Learning: Integrating Temporal Abstraction and Intrinsic Motivation. In *NeurIPS*, 3675–3683.
- Lang, K. J.; Pearlmutter, B. A.; and Price, R. A. 1998. Results of the Abbadingo One DFA Learning Competition and a New Evidence-driven State Merging Algorithm. In *Grammatical Inference*, volume 1433 of *LNCS*, 1–12. Springer.
- Lavaei, A.; Somenzi, F.; Soudjani, S.; Trivedi, A.; and Zamani, M. 2020. Formal Controller Synthesis for Continuous-space MDPs via Model-free Reinforcement Learning. In *International Conference on Cyber-Physical Systems*, 98–107. IEEE.
- Liu, W.; Wei, L.; Sharpnack, J.; and Owens, J. D. 2019. Unsupervised Object Segmentation with Explicit Localization Module. *arXiv* 1911.09228.
- Mao, H.; Alizadeh, M.; Menache, I.; and Kandula, S. 2016. Resource Management with Deep Reinforcement Learning. In *ACM Workshop on Networks*, 50–56. ACM.
- Memarian, F.; Xu, Z.; Wu, B.; Wen, M.; and Topcu, U. 2020. Active Task-Inference-Guided Deep Inverse Reinforcement Learning. In *59th IEEE Conference on Decision and Control, CDC*, 1932–1938. IEEE.
- Mnih, V.; et al. 2015. Human-level Control Through Deep Reinforcement Learning. *Nature* 518(7540): 529–533.
- Ng, A. Y.; Harada, D.; and Russell, S. 1999. Policy Invariance Under Reward Transformations: Theory and Application to Reward Shaping. In *ICML*, volume 99, 278–287.
- Polydoros, A. S.; and Nalpantidis, L. 2017. Survey of Model-based Reinforcement Learning: Applications on Robotics. *Journal of Intelligent & Robotic Systems* 86(2): 153–173.
- Precup, D. 2001. *Temporal Abstraction in Reinforcement Learning*. Ph.D. thesis, University of Massachusetts Amherst.
- Rens, G.; and Raskin, J.-F. 2020. Learning Non-Markovian Reward Models in MDPs. *arXiv* 2001.09293.
- Rens, G.; Raskin, J.-F.; Reynouard, R.; and Marra, G. 2020. Online Learning of Non-Markovian Reward Models. *arXiv* 2009.12600.
- Riedmiller, M. 2005. Neural Fitted Q iteration – First Experiences with a Data Efficient Neural Reinforcement Learning Method. In *ECML*, volume 3720, 317–328. Springer.
- Ryan, R. M.; and Deci, E. L. 2000. Intrinsic and Extrinsic Motivations: Classic Definitions and New Directions. *Contemporary Educational Psychology* 25(1): 54–67.
- Sadigh, D.; Kim, E. S.; Coogan, S.; Sastry, S. S.; and Seshia, S. A. 2014. A Learning Based Approach to Control Synthesis of Markov Decision Processes for Linear Temporal Logic Specifications. In *Conference on Decision and Control*, 1091–1096. IEEE.
- Silver, D.; Huang, A.; Maddison, C. J.; Guez, A.; Sifre, L.; van den Driessche, G.; Schrittwieser, J.; Antonoglou, I.; Panneershelvam, V.; Lanctot, M.; Dieleman, S.; Grewe, D.; Nham, J.; Kalchbrenner, N.; Sutskever, I.; Lillicrap, T.; Leach, M.; Kavukcuoglu, K.; Graepel, T.; and Hassabis, D. 2016. Mastering the Game of Go with Deep Neural Networks and Tree Search. *Nature* 529: 484–503.
- Sutton, R. S.; and Barto, A. G. 1998. *Reinforcement Learning: An Introduction*, volume 1. MIT Press Cambridge.

- Toro Icarte, R.; Klassen, T. Q.; Valenzano, R.; and McIlraith, S. A. 2018. Teaching Multiple Tasks to an RL Agent using LTL. In *Autonomous Agents and Multiagent Systems*, 452–461.
- Toro Icarte, R.; Waldie, E.; Klassen, T.; Valenzano, R.; Castro, M.; and McIlraith, S. 2019. Learning Reward Machines for Partially Observable Reinforcement Learning. In *NeurIPS*, 15497–15508.
- Ulyantsev, V.; Buzhinsky, I.; and Shalyto, A. 2018. Exact Finite-state Machine Identification from Scenarios and Temporal Properties. *International Journal on Software Tools for Technology Transfer* 20(1): 35–55.
- Ulyantsev, V.; and Tsarev, F. 2011. Extended Finite-State Machine Induction Using SAT-Solver. In *International Conference on Machine Learning and Applications and Workshops*, 346–349.
- Vezhnevets, A.; Mnih, V.; Osindero, S.; Graves, A.; Vinyals, O.; Agapiou, J.; et al. 2016. Strategic Attentive Writer for Learning Macro-actions. In *NeurIPS*, 3486–3494.
- Vezhnevets, A. S.; Osindero, S.; Schaul, T.; Heess, N.; Jaderberg, M.; Silver, D.; and Kavukcuoglu, K. 2017. FeUdal Networks for Hierarchical Reinforcement Learning. In *International Conference on Machine Learning*, 3540–3549.
- Vinyals, O.; Babuschkin, I.; Czarnecki, W. M.; Mathieu, M.; Dudzik, A.; Chung, J.; Choi, D. H.; Powell, R.; Ewalds, T.; Georgiev, P.; Oh, J.; Horgan, D.; Kroiss, M.; Danihelka, I.; Huang, A.; Sifre, L.; Cai, T.; Agapiou, J. P.; Jaderberg, M.; Vezhnevets, A. S.; Leblond, R.; Pohlen, T.; Dalibard, V.; Budden, D.; Sulsky, Y.; Molloy, J.; Paine, T. L.; Gulcehre, C.; Wang, Z.; Pfaff, T.; Wu, Y.; Ring, R.; Yogatama, D.; Wünsch, D.; McKinney, K.; Smith, O.; Schaul, T.; Lillicrap, T.; Kavukcuoglu, K.; Hassabis, D.; Apps, C.; and Silver, D. 2019. Grandmaster Level in StarCraft II Using Multi-agent Reinforcement Learning. *Nature* 1–5.
- Walkinshaw, N. 2018. *MINT Framework Github Repository*. URL <https://github.com/neilwalkinshaw/mintframework>.
- Walkinshaw, N.; and Bogdanov, K. 2008. Inferring Finite-State Models with Temporal Constraints. In *Automated Software Engineering*, 248–257. IEEE.
- Walkinshaw, N.; Bogdanov, K.; Holcombe, M.; and Salahuddin, S. 2007. Reverse Engineering State Machines by Interactive Grammar Inference. In *Working Conference on Reverse Engineering*, 209–218. IEEE.
- Walkinshaw, N.; Taylor, R.; and Derrick, J. 2016. Inferring Extended Finite State Machine Models From Software Executions. *Empirical Software Engineering* 21(3): 811–853.
- Watkins, C. J.; and Dayan, P. 1992. Q-learning. *Machine learning* 8(3-4): 279–292.
- Xu, Z.; Gavran, I.; Ahmad, Y.; Majumdar, R.; Neider, D.; Topcu, U.; and Wu, B. 2020. Joint Inference of Reward Machines and Policies for Reinforcement Learning. In *AAAI*, volume 30, 590–598.
- Yuan, L. Z.; Hasanbeig, M.; Abate, A.; and Kroening, D. 2019. Modular Deep Reinforcement Learning with Temporal Logic Specifications. *arXiv* 1909.11591.
- Zheng, Z.; and Yang, Y. 2021. Rectifying Pseudo Label Learning via Uncertainty Estimation for Domain Adaptive Semantic Segmentation. *International Journal of Computer Vision* (to appear).
- Zhou, Z.; et al. 2017. Optimizing Chemical Reactions with Deep Reinforcement Learning. *ACS Central Science* 3(12): 1337–1344.

Appendix

A The Automata Synthesis Framework vs. State Merge

In this section we compare the automata synthesis algorithm we use to algorithms based on state merging. State merge is the established approach for model generation from traces. Traces are first converted into a Prefix Tree Acceptor (PTA). Model inference techniques are then used to identify pairs of equivalent states to be merged in the hypothesis model. Starting from the traditional kTails (Biermann and Feldman 1972a) algorithm for state merging, several alternatives to determine state equivalence have been proposed over the years (Walkinshaw and Bogdanov 2008). For our experiment we used the MINT (Model INference Technique) (Walkinshaw 2018) tool, which implements different variants of the state merge algorithm, including data classifiers (Walkinshaw, Taylor, and Derrick 2016) to check state equivalence for merging.

We generated models using MINT for all seven tasks for the Minecraft environment and explored different tool configurations to generate a model that best fits the input trace. We observed that although MINT is faster, the automata generated by the tool are either too big (meaning they have a large number of states) or are over-generalised (in extreme cases they only have a single state), depending on the tool configurations. For instance, the smallest model that best fits the traces for Task 5 includes 49 states (Fig. 7), and 14 states for Task 6 (Fig. 8). Here, the ‘start’ label signifies the beginning of a new trace obtained from another instance of random exploration. DeepSynth requires automata that are succinct and accurately represent sequential behaviour observed in the exploration trace to ensure fast and efficient learning. Since state merge algorithms do not produce the most succinct model that fits a given trace, we prefer using the automata synthesis algorithm described in Section 4.

B The Automata Synthesis Framework vs. Learning Reward Machines Using Tabu Search

The line of work presented in (Toro Icarte et al. 2019), referred to as LRM here, uses reward machines learnt from trace data to guide the learning process and is very closely related to our work. In this section we compare the two methodologies. The automata synthesis algorithm (Synth) used in this paper implements online learning. Synth converts the model learning problem into a Boolean Satisfiability (SAT) problem and uses a SAT solver to generate models. SAT solvers, in turn, use a backtracking search algorithm, DPLL (Davis and Putnam 1960), to look for a satisfying assignment to the variables in the Boolean formula. LRM, on the other hand, uses Tabu search to explore and find reward machines from trace data. DPLL is complete and explores the entire search space, as opposed to Tabu search, which is local (Cook and Mitchell 1996). Model completeness and accuracy is important in DeepSynth as the agent performance relies on the automaton to guide learning. The automata generated by Synth are complete in the sense that they capture

all sequential behaviour seen in the trace.

DeepSynth uses traces from random exploration to generate an automaton. In each episode sequential behaviours observed over iterations of exploration are incorporated into the automaton without changing the structure of the automaton inferred in previous episodes. More specifically, when the automata is updated, it will always be just a superset of the previous automata. As such, the Q-networks can continue to be used and updated after a automata is updated. Namely, the only required change is that more Q-networks need to be added and old Q networks can be reused. This is not the case in LRM where Q-networks must be reset and relearned from scratch each time the automata changes. Also, in contrast to LRM (generated using Tabu search) Synth does not require an initial model.

Note that in DeepSynth we only care about positive trace samples (Gold 1978). This essentially allows us to add new traces incrementally to the existing automaton. Thus, whenever the agent discovers a new label, it is added to $\Sigma_{\mathcal{A}}$ and the associated trace is considered as the new accepting trace. So as the agent explores the environment over multiple iterations of DeepSynth, we get longer trace sequences with newly discovered labels. These new labels are added incrementally to the partial model generated in previous iterations. Thus, the model generated represents the sequence of labels (or intrinsic goals) that composes extrinsic rewarding tasks. This allows to incrementally build up the DFA from intrinsically accepting traces to extrinsically accepting traces as in Fig 4.

The graph plots in Fig.9 provide a runtime comparison of the Synth algorithm and LRM for increasing trace length in different benchmarks. To ensure a fair comparison, we use the same three examples used to benchmark the LRM approach here: Cookie, 2-Keys and Symbol Domain. Details on the benchmarks can be found in (Toro Icarte et al. 2019). The graph plots show a linear increase in runtime for LRM as trace length increases. The runtime for Synth on the other hand saturates after an initial increase in runtime, and is much lower compared to LRM. Given a set of observed traces, Synth generates a model from the first trace in the set, then incrementally adds any new behaviour seen in subsequent traces. For smaller trace sets, we see new behaviours being added to the model with each trace sequence in the set, but for larger trace sets subsequent trace sequences do not show any new behaviours that are not already captured by the automaton. Therefore, the runtime saturates once all behaviours are captured by the generated automaton. The minimal noise observed in the runtime plots can be attributed to trace processing and plotting the generated automaton.

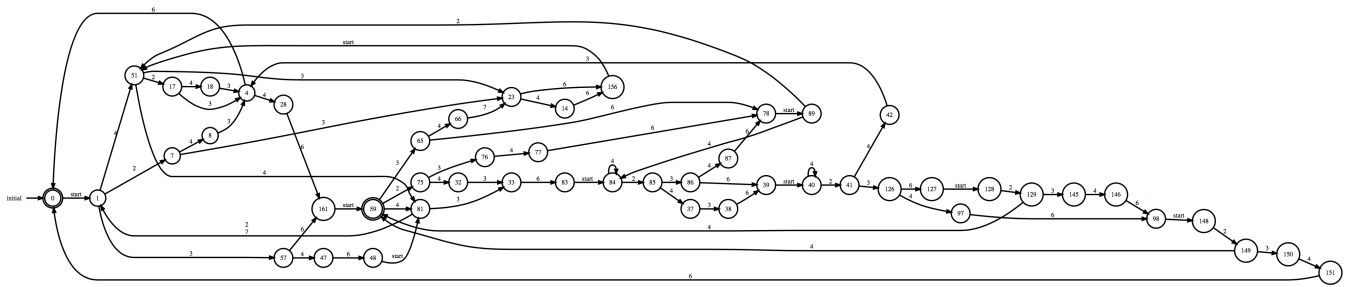


Figure 7: Best fit model for Task 5 generated by the MINT tool.

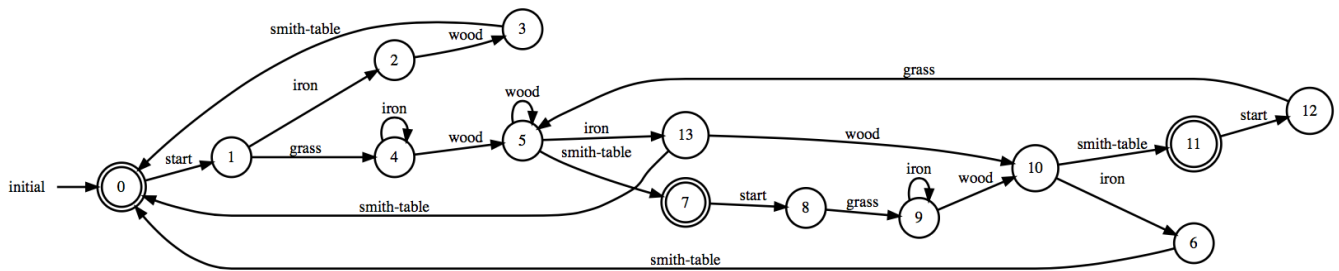


Figure 8: Best fit model for Task 6 generated by the MINT tool.

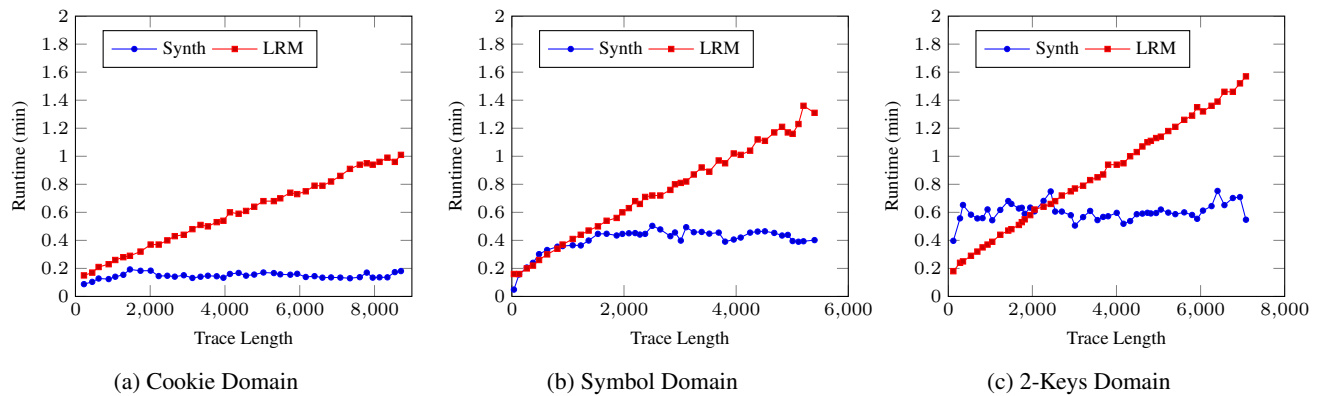
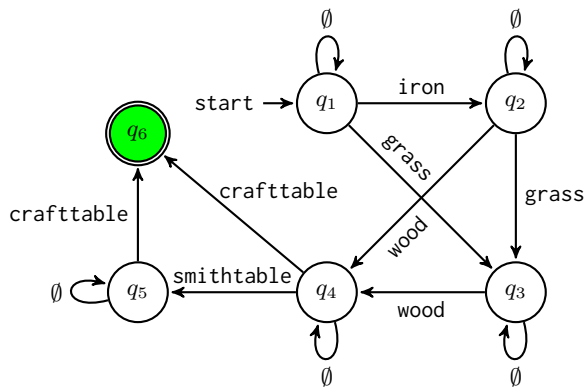
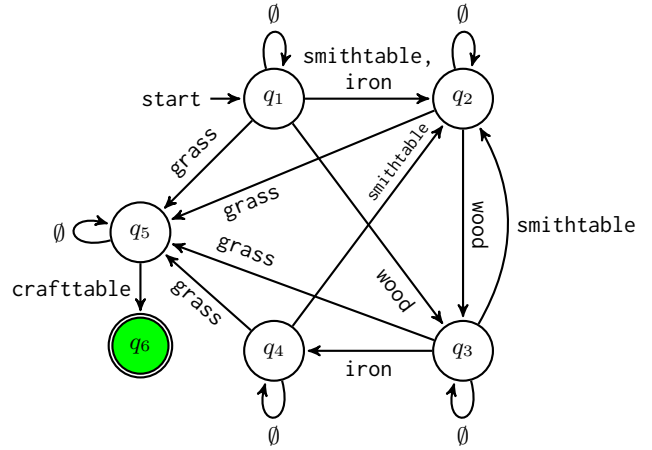


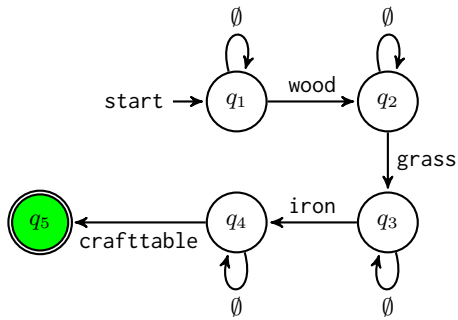
Figure 9: Runtime comparison of Tabu search vs. the Synth algorithm.



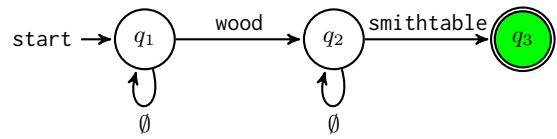
(a) Task 1



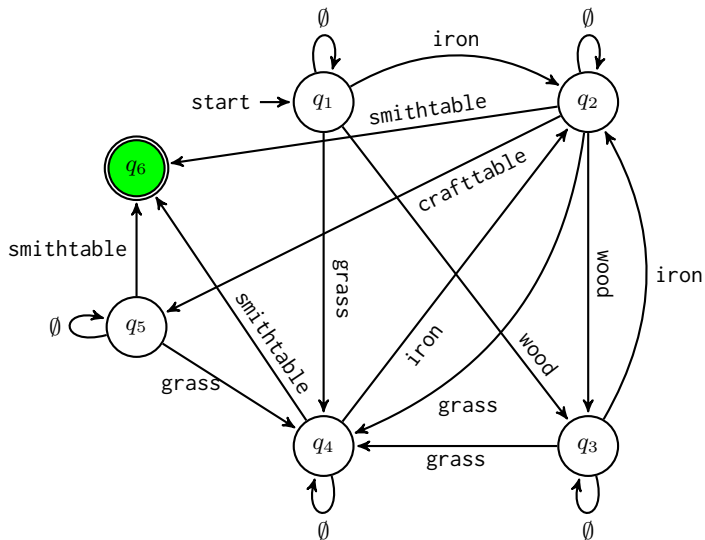
(b) Task 2



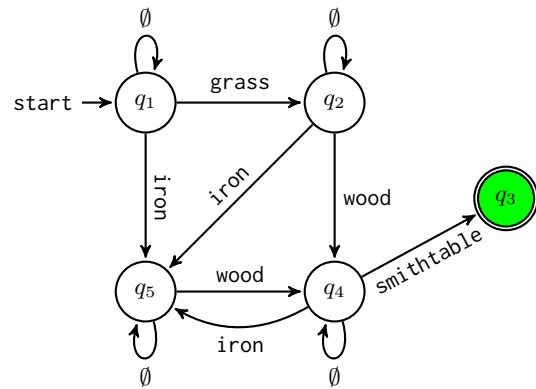
(c) Task 3



(d) Task 4



(e) Task 5



(f) Task 6

Figure 11: Automata generated for the Minecraft Tasks 1 to 6

Task	Sequence
Task1	Σ^* wood Σ^* craft table
Task2	Σ^* grass Σ^* craft table
Task3	Σ^* wood Σ^* grass Σ^* iron Σ^* craft table
Task4	Σ^* wood Σ^* smith table
Task5	Σ^* grass Σ^* smith table
Task6	Σ^* iron Σ^* wood Σ^* smith table
Task7	Σ^* wood Σ^* iron Σ^* craft table Σ^* gold

Table 2: High-level sequence for each task

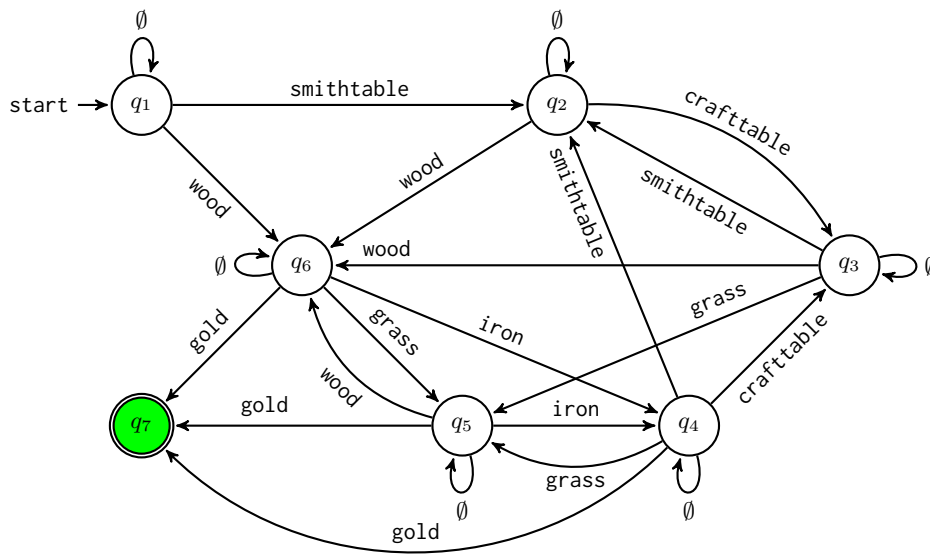


Figure 12: Automaton generated for the Minecraft Task 7

reward is back-propagated to the second and so on. Other networks associated with automaton states within non-optimal paths remained unstable and are not shown. In both tasks, each NFQ module includes 2 hidden layers and 128 ReLUs.

The crafting environment outputs a reward for Task 1 when the agent brings “wood” to the “craft table”. Fig. 14a illustrates the results of training for Task 1. Note that with the very same training set \mathcal{E} of 4500 training samples DeepSynth is able to converge while DQN fails. Task 3 has a more complicated sequential structure, as given in Table 2. An example policy learnt by DeepSynth for Task 3 is provided in Fig. 2. Fig. 14b gives the result of training for Task 3 using DeepSynth and DQN where the training set \mathcal{E} has 6000 training samples. However, for Task 3, DQN failed to converge even after we increased the training set by an order of magnitude to 60000.

Montezuma’s Revenge

In Montezuma’s Revenge, the emulator’s internal state is not visible to the agent. The agent only observes an image, which is a matrix of pixel values that represent the current screen. Inspired by (Mnih et al. 2015), we apply a basic pre-processing step to the Atari 2600 frames, designed to reduce the dimensionality of the input. We extract the luminance from the RGB frame and rescale it to 84×84 . Further, a grey-scaling pre-processing is applied and then the 4 most recent frames are stacked together to form the input to a DQN module.

The agent selects and executes actions according to an ϵ -greedy policy. Similar to the NFQ, the DQN module also uses experience replay, which averages the behaviour distribution over many of previous states, smoothing out learning and avoiding oscillations or divergence in the parameters (Riedmiller 2005; Mnih et al. 2015). Each DQN module stores a finite number of last experience tuples in the replay memory, and samples minibatches uniformly at random. Further, to improve the stability of the deep nets, we use a separate network in each module for generating the target y values in (4). Specifically, after a finite number of steps we clone the module network to obtain a target network, which is used to generate the Q-learning targets y . This modification makes the algorithm more stable compared to standard QL and NFQ

Algorithm 2: DeepSynth with Temporal DQN

```

input : automaton  $\mathfrak{A}$  from the Synth step
output : approximated optimal  $Q$ -function:  $\hat{Q}^*$ 
1 initialise all neural nets  $B_{q_i}$  with random weights
2 repeat
3   initialise the state to  $(s_0, q_0)$ 
4   for  $t = 1, total\_time\_steps$  do
5      $a_t = \arg \max_a B_{q_t}$  with  $\epsilon$ -greedy
6     execute action  $a_t$  and observe the total reward  $r_t^T$ 
7     observe the next image  $s_{t+1}$ 
8     semantic segmentation outputs  $L(s_{t+1})$ 
9     update the automaton state from  $q_t$  to  $q_{t+1}$ 
10    preprocess images  $s_t$  and  $s_{t+1}$  to  $\mathcal{P}_t$  and  $\mathcal{P}_{t+1}$ 
11    store transition  $(\mathcal{P}_t, a_t, \mathcal{P}_{t+1}, r_t^T, L(s_{t+1}))$  in  $\mathcal{E}_{q_t}$ 
12    sample minibatch from  $\mathcal{E}_{q_t}$ 
13    target value from target network  $\hat{B}_{q_t}$ ,
         $y_i = r_i^T + \gamma \max_{a'} Q(\mathcal{P}_{i+1}, a' | \theta^{\hat{B}_{q_t}})$ 
14    update  $B_{q_i}$  weights using  $y_i$ 
15    clone the current network  $B_{q_i}$  to  $\hat{B}_{q_t}$  every  $C$  steps
16  end
17 until end of trial

```

updates (Mnih et al. 2015).

An overview of the algorithm is presented as Algorithm 2. The values of all the hyper-parameters and descriptions of all hyper-parameters are provided in Table 3.

Algorithm 1: DeepSynth with Temporal NFQ

```

input : automaton  $\mathfrak{A}$  from the Synth step,
        the set of transition samples  $\mathcal{E}$ 
output : approximated optimal  $Q$ -function:  $\hat{Q}^*$ 
1 initialize all neural nets  $B_{q_i}$  with random weights
2 repeat
3   for  $q_i = |\mathcal{Q}|$  to 1 do
4      $\mathcal{P}_{q_i} = \{(input_l, target_l), l = 1, \dots, |\mathcal{E}_{q_i}|\}$ 
5      $input_l = (s_l, a_l)$ 
6      $target_l = R^T(s_l, a_l) + \gamma \max_{a'} Q(s'_l, a')$ 
7     where  $(s_l, a_l, s'_l, r^l, L(s'_l)) \in \mathcal{E}_{q_i}$ 
8      $B_{q_i} \leftarrow \text{Adam}(\mathcal{P}_{q_i})$ 
9   end
10 until end of trial

```

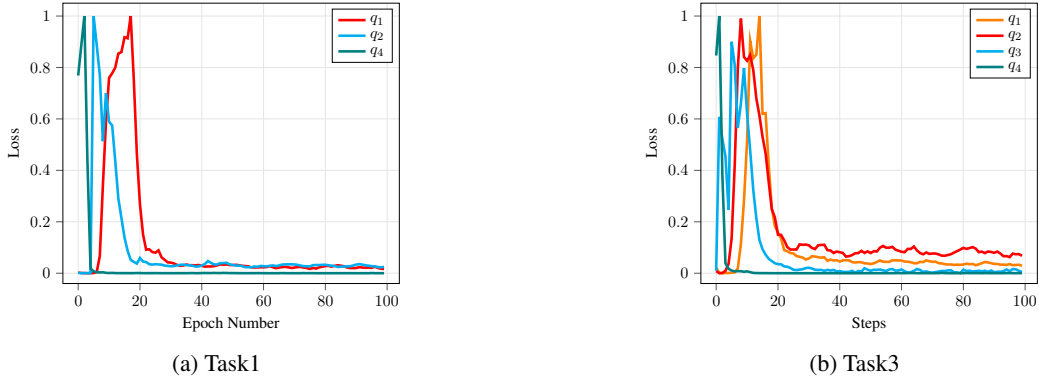


Figure 13: Training progress for Tasks 1 and 3 with three and four active hybrid deep NFQ modules coupled together, respectively.

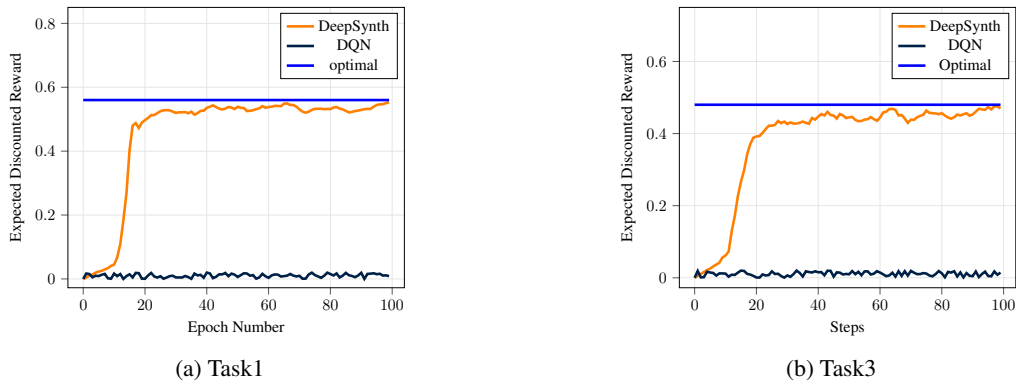


Figure 14: Training progress for Tasks 1 and 3 with DeepSynth and DQN on the same training set \mathcal{E} . The expected return is over state $s_0 = [4, 4]$ with origin being the bottom left corner cell.

Hyperparameter	Value	Description
minibatch size	32	Number of training cases over which each Stochastic Gradient Descent (SGD) update is computed
replay memory size	150000	SGD updates are sampled from this number of most recent frames.
agent history length	4	The number of most recent frame experienced by the agent that are given as input to the Q network
target network update frequency	10000	The frequency (measured in the number of parameter updates) with which the target network is updated
discount factor	0.99	Discount factor gamma used in the Q-learning update
learning rate	0.00025	The learning rate used by RMSProp
initial exploration	1	Initial value of ϵ in ϵ -greedy exploration
final exploration	0.1	Final value of ϵ in ϵ -greedy exploration
final exploration frame	150,000	The number of frames over which the initial value of ϵ is linearly annealed to its final value
replay start size	8000	A uniform random policy is run for this number of frames before learning starts and the resulting experience is used to populate the replay memory.
no-op max	30	Maximum number of “do nothing” actions to be performed by the agent at the start of an episode.

Table 3: Hyper-parameters of the DQN Modules for Montezuma’s Revenge

D Automata Synthesised for Other Benchmarks

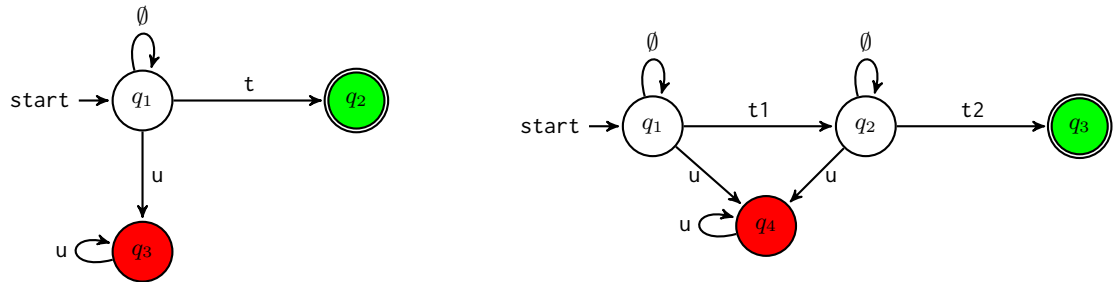


Figure 15: Automata synthesised for mars-rover-1 and mars-rover-2

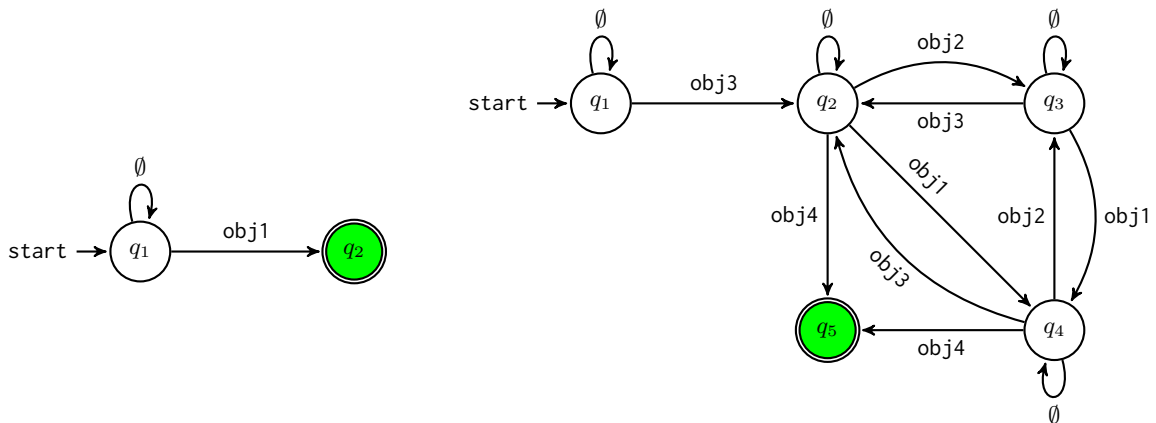


Figure 16: Automata synthesised for slp-easy and slp-hard.

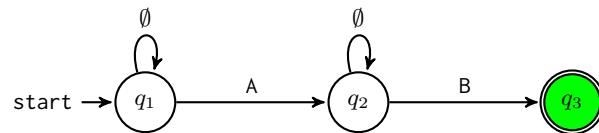


Figure 17: Automaton synthesised for robot-surve.

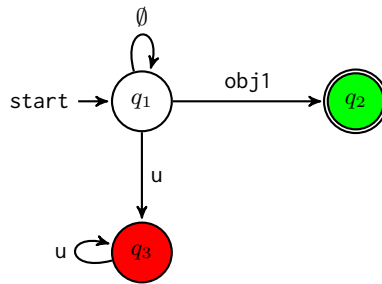


Figure 18: Automaton synthesised for frozen-lake-1, 2, 3.

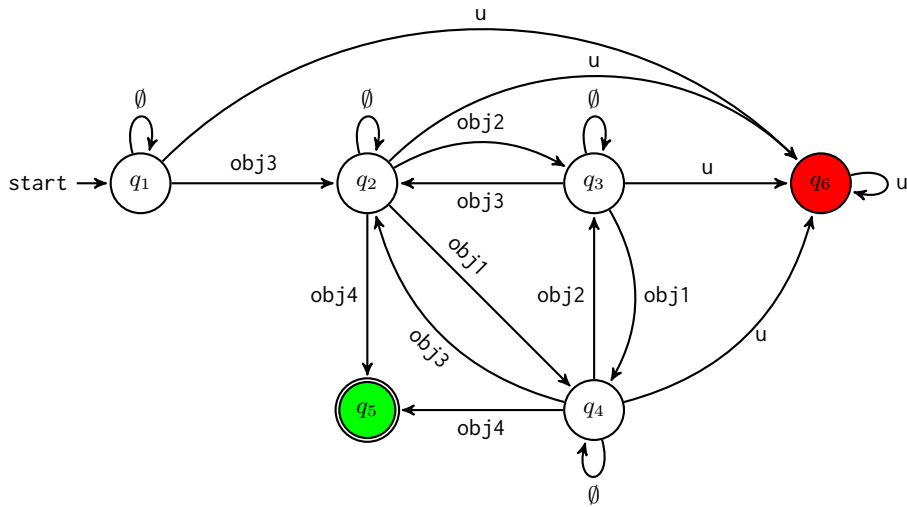


Figure 19: Automaton synthesised for frozen-lake-4, 5, 6.